

Analysis of first overtone bands of isotopologues of CO and SiO in stellar spectra

Ya. V. Pavlenko^{1,3}, Sergei N. Yurchenko², and Jonathan Tennyson²

¹ Main Astronomical Observatory of NAS Ukraine, 27 Zabolotnoho, Kyiv, 01137, Ukraine

² Department of Physics and Astronomy, University College London, London WC1E 6BT, United Kingdom

³ Centre for Astrophysics Research, University of Hertfordshire, College Lane, Hatfield, AL10 9AB, United Kingdom

November 28, 2019

ABSTRACT

Context. The first overtone ($\Delta v = 2$) bands of the monosubstituted isotopologues of CO at $2.3 \mu\text{m}$ in the spectrum of Arcturus (K2 III), and of the monosubstituted isotopologues of SiO at $4 \mu\text{m}$ in the spectrum of the red giant HD196610 (M6 III) are modelled.

Aims. To investigate problems involving the computation of the first overtone bands of isotopologues of CO and SiO in spectra of late-type stars and to determine isotopic abundances.

Methods. We use fits of theoretical synthetic spectra to the observed stellar molecular bands of CO and SiO to determine abundances of isotopes of C, O and Si.

Results. Fits of synthetic spectra of the $^{12}\text{C}^{16}\text{O}$ first overtone bands at $2.3 \mu\text{m}$ computed with three available line lists (Goorvitch, HITEMP2010 and Li *et al.*) to the observed spectrum of Arcturus provide the same carbon abundance $[\text{C}] = -0.6$ and isotopic ratio of carbon $^{12}\text{C}/^{13}\text{C} = 10 \pm 2$. However, the quality of fits to the observed spectrum differ for three line lists used. Furthermore, the derived oxygen isotopic ratio $^{16}\text{O}/^{18}\text{O} = 2000 \pm 500$ is larger than that known in the solar system where $^{16}\text{O}/^{18}\text{O} = 500$. The silicon isotopic ratio in the atmosphere of the red giant HD196610 is revised. Using the ExoMol SiO line list with appropriate statistical weights for the SiO isotopologues the ‘non-solar’ ratio $^{28}\text{Si}:^{29}\text{Si}:^{30}\text{Si} = 0.86 \pm 0.03:0.12 \pm 0.02:0.02 \pm 0.01$ is obtained.

Conclusions. We found that a) the computed isotopic carbon and silicon ratios determined by the fits to the observed spectrum depend on the adopted abundance of C and Si, respectively; b) Correct treatment of the nuclear spin degeneracies parameter is of crucial importance for the use of nowadays HITRAN/ExoMol line lists in the astrophysical computations.

1. Introduction

Carbon has 15 known isotopes, from ^8C to ^{22}C , of which ^{12}C and ^{13}C are stable. When a main-sequence star enters the red-giant branch, some convective mixing processes occur in its interiors that carry nuclei affected by CN cycling from internal layers to the surface, see Sneden (1991); Charbonnel & Zahn (2007). Theory predicts a decrease in the $^{12}\text{C}/^{13}\text{C}$ ratio with respect to the main sequence value (~ 89 in the case of the Sun), down to values in the range 15 – 30, depending on the initial mass and metallicity of the star, see Charbonnel & Zahn (2007). Subsequently, the carbon abundance in the outer layers of red giants drops, and nitrogen increases.

There are three known stable isotopes of oxygen: ^{16}O , ^{17}O , and ^{18}O . Radioactive isotopes ranging from ^{11}O to ^{26}O have also been characterized, all short-lived. If the stellar mass of a red giant does not exceed $1.3 M_{\odot}$, the ^{16}O abundance remains unaltered, while that of ^{18}O is mildly reduced, see Palmerini *et al.* (2011). In higher-mass stars, the dominant energy production process is the CNO cycle, which is a catalytic cycle that uses nuclei of carbon, nitrogen and oxygen as intermediaries and in the end produces a helium nucleus as with the proton-proton chain (Böhmer-Vitense 1992). However, in all cases the carbon and oxygen isotopic ratios depend on the initial stellar masses and abundances (Charbonnel & Zahn 2007), so these pa-

rameters are of crucial importance for understanding stellar evolution.

Silicon has 23 known isotopes, with mass numbers ranging from 22 to 44. ^{28}Si (the most abundant isotope), ^{29}Si , and ^{30}Si are stable. All three stable isotopes of silicon are produced in stars through the oxygen-burning process, with the most abundant ^{28}Si being made as part of the α -process. Oxygen-burning in massive stars larger than $10.3 M_{\odot}$ is preceded by the neon-burning process, although ^{16}O is lighter than neon; oxygen in stars of lower masses cannot ignite. After completing the oxygen burning processes the core of a star is primarily composed of silicon and sulfur, see Clayton (1983); Hirschi (2014); Caughlan & Fowler (1988), and references therein. At advanced stages of massive star evolution the core oxygen-burning process is succeeded by the fusion of ^{28}Si with α -particles prior to a violent type II supernova event, see Nakamura *et al.* (1999).

It is worth noting that carbon, oxygen and silicon isotopes form in very specific and different nuclear reactions. Knowledge of the isotopic composition of stars is therefore important for our understanding of how the Universe works, see Romano *et al.* (2017).

Unfortunately, determination of isotopic abundances of C, O, Si from analysis their absorption lines in the optical spectral region is complicated by the small wavelength shifts of the corresponding lines and the effects of blending which increase significantly with lower effective stellar tem-

arXiv:1911.12326v1 [astro-ph.SR] 27 Nov 2019

peratures. Fortunately, molecular line positions shift significantly with isotopic substitution and the infrared bands of different isotopologues in stellar spectra can provide input for the analysis of isotopic abundances.

Vibrational bands of CO and SiO isotopologues are observed in spectra of late-type stars with the first overtone ($\Delta v = 2$) bands having similar shapes. However, due to the larger mass of the SiO molecule its fundamental rovibrational spectrum is redder at $4 \mu\text{m}$ with respect to the bands of CO located at $2.3 \mu\text{m}$.

Furthermore, because of its large dissociation energy and the relatively high abundance of its constituent atoms, carbon monoxide in its several isotopic forms is observed in a variety of astrophysical sources, including erupting supernovae, stellar photospheres, comets, and the interstellar medium, see e.g., Romano et al. (2017), Iwagami et al. (2015), Banerjee et al. (2018), and references therein.

Silicon monoxide, SiO, is an important constituent of these astrophysical environments. The millimetre-range maser lines of SiO have been extensively used in the astrophysical applications, see Tobin et al. (2019), Vlemmings et al. (2011), and Yoon et al. (2014) for more details. Thermal lines of SiO in the sub-mm and mm spectral ranges have also been studied extensively as a probe of circumstellar dust formation, conspicuous axial symmetry and bipolar dynamics, see González Delgado et al. (2003) for AGB stars and de Vicente et al. (2016) for a variety of evolved stars, as well as references therein.

The fundamental band of SiO was identified in the spectra of M supergiants a long time ago (Knacke et al. 1969; Rinsland & Wing 1982; Wollman et al. 1973). The strong $4 \mu\text{m}$ band of SiO appears in the spectra of cooler stars, at least up to the spectral type M6. The first overtone band of SiO forms notable structures in the observed spectra of late-type stars, see Evans et al. (2019), and Pavlenko (2019) for more details. Furthermore, some recent theoretical studies of hot and dense atmospheres of exoplanets suggest the possible presence of significant amounts of SiO and other silicates (Schaefer et al. 2012; Tinetti et al. 2018).

In this work we obtain isotopic ratios for carbon, oxygen and silicon by analyzing spectra of two cool stars, namely, Arcturus (K2 III) and HD196610 (M6 III). Strictly speaking, we use Arcturus as a template star with known fundamental parameter to fit our synthetic spectra computed with the different line lists of various isotopologues of CO to the observed stellar spectra. In other words, a secondary aim of this paper is to compare different CO and SiO line lists for the analysis of the isotopic abundance of stellar atmospheres and to demonstrate the importance of the consistent treatment of the molecular statistical weights when computing molecular opacity and partition functions.

2. Line lists

In the following we analyse different line lists for monosubstituted isotopologues of CO and SiO available in the literature: the three line lists for CO by Goorvitch (1994), HITEMP2010 (Rothman et al. 2010) and HITRAN2018 by Li et al. (2015) and an SiO line list by Barton et al. (2013).

2.1. CO by Goorvitch (1994)

Goorvitch (1994) computed carbon monoxide line lists for seven isotopologues, namely $^{12}\text{C}^{16}\text{O}$, $^{13}\text{C}^{16}\text{O}$, $^{12}\text{C}^{17}\text{O}$,

$^{12}\text{C}^{18}\text{O}$, $^{13}\text{C}^{18}\text{O}$, $^{14}\text{C}^{16}\text{O}$, and $^{13}\text{C}^{17}\text{O}$, containing rotation-vibration transitions of the fundamental, first, and second overtone bands up to $v = 20$ and $J = 149$, as well as pure rotational transitions for up to $v = 5$ and $J = 60$, of the ground electronic state $X^1\Sigma^+$. The transitions dataset provided by Goorvitch (1994) comes with the transition frequencies, the lower state energies, the Einstein A-values, the R-values, the expectation value of the effective dipole moment operator, and the quantum numbers of each transition.

2.2. CO in HITEMP2010

The HITEMP2010 list list for CO isotopologues (Rothman et al. 2010) is in fact, the modified CO line list from HITEMP1995 in which the data were assembled from the line list of Goorvitch (1994). These changes are described by Rothman et al. (2010) as “The only exception is where there have been updates to the line parameters in HITRAN for carbon monoxide after 1995; in these cases the improved values were adopted for the HITEMP2010 compilation.” Nevertheless, we were interested to see whether these updates of the CO line list would change the results of the carbon isotope determination.

2.3. CO by Li et al. (2015)

Li et al. (2015) computed new extensive rovibrational line lists for nine isotopologues $^{12}\text{C}^{16}\text{O}$, $^{13}\text{C}^{16}\text{O}$, $^{12}\text{C}^{17}\text{O}$, $^{14}\text{C}^{16}\text{O}$, $^{13}\text{C}^{17}\text{O}$, $^{13}\text{C}^{18}\text{O}$, $^{14}\text{C}^{16}\text{O}$, $^{14}\text{C}^{17}\text{O}$, and $^{14}\text{C}^{18}\text{O}$ in the ground electronic state with $v < 42$, $\Delta v < 12$, and $J < 151$. These line lists were subsequently included in HITRAN2016 (Gordon et al. 2017). The line intensity and position calculations were computed using a newly determined piece-wise dipole moment function (DMF) in conjunction with wavefunctions calculated using an empirically determined potential energy function by Coxon & Hajigeorgiou (2013). A direct fit method that simultaneously fits all the reliable experimental rovibrational intensities was used to construct the DMF of CO at internuclear distances near equilibrium. Li et al. (2015) claimed that molecular constants used to construct their line list, including those generated by Coxon & Hajigeorgiou (2004), are accurate enough to reproduce all relevant spectroscopic line positions to the same degree of precision as that achieved in the direct potential fit.

2.4. SiO by Barton et al. (2013)

The EBJT line lists for silicon monoxide were computed by Barton et al. (2013) as part of the ExoMol project (Tennyson & Yurchenko 2012) for the main isotopologue, $^{28}\text{Si}^{16}\text{O}$, and for four monosubstituted isotopologues ($^{29}\text{Si}^{16}\text{O}$, $^{30}\text{Si}^{16}\text{O}$, $^{28}\text{Si}^{18}\text{O}$ and $^{28}\text{Si}^{17}\text{O}$), in their ground electronic states. These line lists are suitable for high temperatures (up to 9000 K), including those relevant to exoplanetary atmospheres, cool stars and sunspots. Barton et al. (2013) used a combination of empirical and ab initio methods: the potential energy curves were determined to high accuracy by fitting to extensive data from the analysis of both laboratory and sunspot spectra; a high-quality ab initio dipole moment curves were calculated at the large

basis set, with account of multireference configuration interactions.

2.5. ‘Physics’ and ‘astrophysics’ conventions of the nuclear statistical weights and partition functions

Two main conventions for definition of the nuclear statistical weights and associated partition functions Q exist: the ‘physics’ and ‘astrophysics’ conventions. Their use requires special care when using line lists for astrophysical applications. Let us consider an absorption coefficient (line intensity) $I_{f \leftarrow i}$ for a transition from an initial i to a final state f as given in SI units, see Bernath (2015):

$$I(f \leftarrow i) = \frac{e^2}{4\epsilon_0 m_e} \frac{g_i f_{if} e^{-E_i/kT}}{Q} [1 - \exp(-hc\tilde{\nu}_{if}/kT)], \quad (1)$$

where f_{if} is an oscillator strength, for the transition from the state i with energy E_i , in thermal equilibrium at the temperature T , to the state f with energy E_f , $\tilde{\nu}_{if}$ as the transition wavenumber, $hc\tilde{\nu}_{if} = E_f - E_i$, m_e is the electron mass, e is the electron charge, k is the Boltzmann constant, g_i is the degeneracy of the (lower) state i , ϵ_0 is the permittivity of free space and, finally, Q is the partition function, given by

$$Q = \sum_i g_i e^{-E_i/kT}. \quad (2)$$

The statistical factor g_i according to the ‘astrophysics’ convention, commonly adopted by astronomers, is given by

$$g_i = (2J_i + 1) \frac{g_i^{(\text{ns})}}{\bar{g}^{(\text{ns})}}, \quad (3)$$

where $g_i^{(\text{ns})}$ is the nuclear spin degeneracy of the state in question and $\bar{g}^{(\text{ns})}$ is the ‘total’ nuclear spin factor. Examples of the partition functions Q computed using this convention include works by Irwin (1981) and Sauval & Tatum (1984). According to the ‘physics’ convention, the statistical weight g_i is the total degeneracy of the state i :

$$g_i = (2J_i + 1) g_i^{(\text{ns})}. \quad (4)$$

This definition is adopted by major databases such as HITRAN (Gamache et al. 2017), ExoMol (Tennyson et al. 2016) and JANAF (Chase & et al. 1985). As one can see from Eqs. (2) and (3), the factor $\bar{g}^{(\text{ns})}$ appears both in the numerator and denominator of Eq. (1) and thus cancels, i.e. both conventions give identical intensities, providing their consistent usage both in Q and $I(f \leftarrow i)$. However, this difference is a common source of errors when the conventions used for the intensities (oscillator strength) and partition functions are mixed up, leading to non-physical results.

To convert between conventions:

$$g_i f_{if}^{(\text{astro})} = \frac{g_i f_{if}^{(\text{phys})}}{\bar{g}^{(\text{ns})}}. \quad (5)$$

As a very typical illustration, the nuclear spin degeneracies of the ortho and para states of water are $g_{\text{ortho}}^{(\text{ns})} = 3$ and $g_{\text{para}}^{(\text{ns})} = 1$. Thus, the corresponding ‘astrophysics’ spin factors are 3/4 and 1/4 respectively (4 is the sum of $g_{\text{ortho}}^{(\text{ns})}$

Table 1. Carbon, oxygen and silicon atom nuclear spin degeneracy parameters

Atom	I	$2I + 1$
^{12}C	0	1
^{13}C	1/2	2
^{14}C	0	1
^{16}O	0	1
^{17}O	5/2	6
^{18}O	0	1
^{28}Si	0	1
^{29}Si	1/2	2
^{30}Si	0	1

and $g_{\text{ortho}}^{(\text{ns})}$), while the ‘physics’ spin factors coincide with the nuclear spin degeneracies $g_{\text{ortho}}^{(\text{ns})}$ and $g_{\text{para}}^{(\text{ns})}$. Hence, the ‘astrophysics’ and ‘physics’ partition functions are related as

$$\frac{Q^{(\text{phys})}}{Q^{(\text{astro})}} = 4.$$

The wrong usage of the conventions can lead to the intensities being too strong or too weak by the factor of 4.

The nuclear spin degeneracy of a heteronuclear diatomic molecule AB molecule, $g \equiv g_{if}$, is the same for all states and is given by

$$g = (2I(A) + 1)(2I(B) + 1) \quad (6)$$

where $I(X)$ is the nuclear spin of isotope X .

Turning to CO, $^{12}\text{C}^{16}\text{O}$ has zero nuclear spin degeneracy so in this case the factor is unity meaning that ‘physics’ and ‘astronomy’ conventions are the same. The nuclear spin degeneracy factor of $^{13}\text{C}^{16}\text{O}$ is 2 and therefore mixing different conventions in partition functions and oscillator strength would lead to a factor of two difference.

For CO, the Goorvitch (1994) line lists were computed in the framework of the ‘astrophysics’ convention while those of Li et al. (2015) and HITEMP (Rothman et al. 2010), as well as the SiO line lists of Barton et al. (2013), used the ‘physics’ convention. To remain within one system of definitions we recomputed the gf provided by Li et al. (2015), HITEMP2010 and Barton et al. (2013) using the ‘astrophysics’ convention.

3. Spectral models

3.1. Observed spectra

For the analysis, the infrared spectrum of Arcturus obtained by Hinkle et al. (1995) was used. The resolution of the spectrum is of order 100 000 with the spectral lines broadened by the rotation ($v \sin i = 1.5 - 3$ km/s) and macroturbulent motions in its atmosphere ($V_{\text{macro}} \sim 4-6$ km/s).

The HD196610 spectrum, taken from the IRTF stellar spectra library (Rayner et al. 2009), also contains SiO bands. Despite much lower resolution ($R \sim 2000$), the structure of the first overtone bands is very evident.

3.2. Opacities, model atmospheres

For Arcturus we adopt $T_{\text{eff}} = 4200$ K, $\log g = 1.5$, and a set of abundances determined by Peterson et al. (1993), with

$\log N(\text{Fe}) = -4.87$, $\log N(\text{C}) = -3.78$, $\log N(\text{O}) = -3.21$,
 $\log N(\text{Si}) = -4.59$.

For HD196610, the computations were performed for $T_{\text{eff}} = 3500$ K. McDonald et al. (2016) found from analysis of CO and Na equivalent widths the metallicity $[\text{Fe}/\text{H}] = -0.3 - -0.26$, however in their analysis they used lower T_{eff} by ~ 250 K determined by Cesetti et al. (2013) and McDonald et al. (2012). Furthermore, they determined for the star $\log g = 0.39$, see table 3 in McDonald et al. (2016). To show possible effects of metallicity and gravity uncertainties on the results of Si abundance and isotopic ratio determination we carried out our analysis for the cases of $[\text{Fe}/\text{H}] = 0$ and -0.3 , gravities $\log g = 1.0$ and 0.5 . In this paper we adopt the ‘‘solar’’ scale of abundances from Anders & Grevesse (1989): $\log N(\text{C}) = -3.48$, $\log N(\text{O}) = -3.11$, $\log N(\text{Si}) = -4.49$, but for iron we adopt $\log N(\text{Fe}) = -4.54$ from Asplund et al. (2009).

Atomic lines from VALD3 (Ryabchikova et al. 2015), as well as molecular lines of H_2O , TiO , CrH , VO , CaH , $^{12}\text{C}^{16}\text{O}$ and $^{13}\text{C}^{16}\text{O}$ were accounted in the 1D model atmosphere computations by SAM12, see more details in Pavlenko (2003). Synthetic spectra were computed for a 1D model atmosphere using the WITA6 program (Pavlenko 1997) assuming Local Thermal Equilibrium (LTE). Our model atmosphere and synthetic spectra were computed for the microturbulent velocity of $V_t = 1.7$ km/s.

3.3. Synthetic spectra

The synthetic spectra were computed using program WITA6 within a classical framework, e.g. LTE, hydrostatic equilibrium and a one-dimensional model atmosphere without sources and sinks of energy. Theoretical synthetic spectra were computed across the first overtone bands of CO (22500–22500 Å) and SiO (39000–42000 Å) with a wavelength step 0.05 Å, opacities due to absorption by atoms, and H_2O were also accounted for.

3.4. Fits to the observed spectra

The best fit to the observed spectra was achieved by the χ^2 procedure described elsewhere (Pavlenko 2014). We give a few details here to aid understanding of the procedure. As part of the fit, the function

$$S = \sum_{i=1}^N s_i^2$$

is minimized, where $s_i = |F_i^{\text{obs}} - F_i^{\text{comp}}|$; F_i^{obs} and F_i^{comp} are the observed and computed fluxes, respectively, and N is the number of the wavelengths points used in the minimisation procedure. In our analysis we omit some spectral ranges which contain artifacts provided by strong noise, telluric absorption, bad pixels, etc. The minimisation factor S is computed on a 3D grid of radial velocity sets, normalisation factors, and broadening parameters. The errors of the fit is evaluated as $\delta = \sum s_i/N$. In some of the plots, the errors δ are indicated as error bars for S .

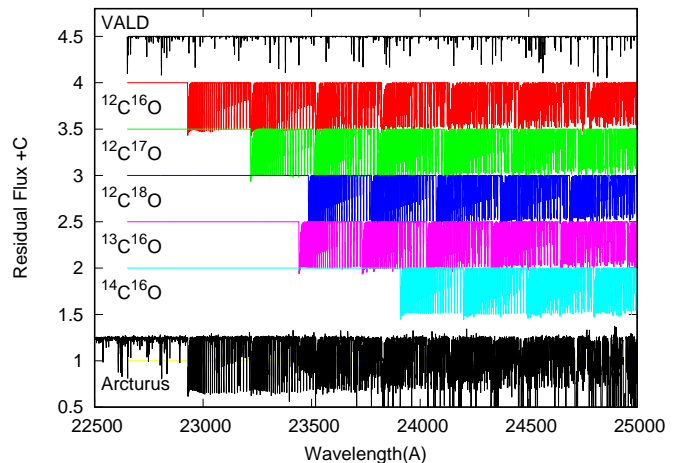


Fig. 1. Positions of the CO isotopologue bands in the observed spectrum of Arcturus due to Hinkle et al. (1995). Atomic absorption lines from VALD (Ryabchikova et al. 2015) across the spectral region are also shown.

4. Results

4.1. Identification of isotopic CO bands

The CO first overtone bands system covers a wide spectral range. Here we restrict our analysis at 22 360–25 000 Å. To verify the consistency of our results with Pavlenko (2008), the carbon abundance and carbon $^{12}\text{C}/^{13}\text{C}$ isotopic ratio were determined for a narrower spectral range of 23 600–23 800 Å, which contains several molecular bands of the CO monosubstituted isotopologues.

The positions of the first overtone bands of the CO isotopologues in the observed spectrum of Arcturus is shown in Fig. 1. We note the distinct wavelength differences in locations of $^{12}\text{C}^{16}\text{O}$, $^{12}\text{C}^{18}\text{O}$, $^{13}\text{C}^{16}\text{O}$, $^{14}\text{C}^{16}\text{O}$ band heads, with the $^{12}\text{C}^{17}\text{O}$ and $^{12}\text{C}^{16}\text{O}$ band heads overlapping. All molecular lists, except for $^{14}\text{C}^{16}\text{O}$, were taken from the HITEMP database, while the line list for $^{14}\text{C}^{16}\text{O}$ was taken from Li et al. (2015).

4.2. Carbon abundance and $^{12}\text{C}/^{13}\text{C}$ in Arcturus

It is worth noting that CO absorption dominates the spectrum of Arcturus across the fitted spectral region, and that absorption by H_2O is very weak in this region. We therefore exclude H_2O from our analysis for the Arcturus data.

The carbon abundance and the carbon isotopic ratio were determined iteratively, using line lists by Goorvitch (1994); Rothman et al. (2010); Li et al. (2015). For any new carbon abundance model the atmosphere of Arcturus was recomputed, resulting in $\log N(\text{C}) = -3.78 \pm 0.1$ and $^{12}\text{C}/^{13}\text{C} = 10 \pm 2$, respectively, for all three line lists. Our fitting procedure ignores the ‘bad’ spectral features, likely created by telluric absorption lines, see Hinkle et al. (1995). These features are marked by thick blue lines in Fig. 2 where the results of the fits to the observed spectrum are shown. We note that our carbon abundance $\log N(\text{C}) = -3.78$ agrees within the error bar with the values found using a different procedure by Peterson et al. (1993), Ryde et al. (2009), and Abia et al. (2012).

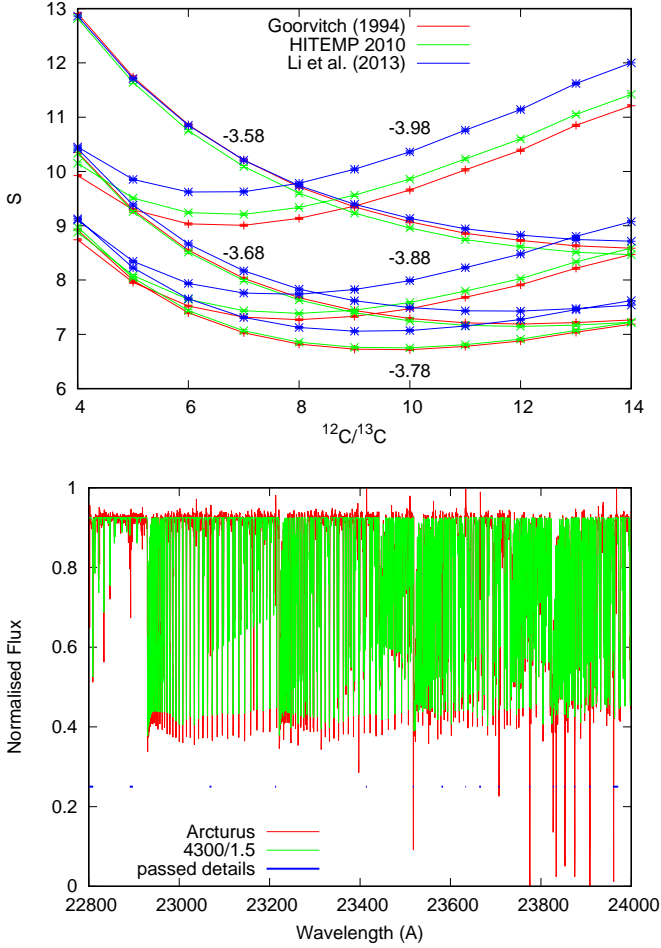


Fig. 2. *Upper panel:* Dependence of the minimisation parameter S computed for different line lists on the carbon abundance in the atmosphere of Arcturus. The adopted carbon abundance is shown above the correspondent curve. *Lower panel:* Best fit to the observed spectrum computed with $\log N(C) = -3.78$ and $^{12}\text{C}/^{13}\text{C} = 10$. Spectral ranges containing artifacts which were missed by minimisation procedure are marked by thick blue lines.

4.3. $^{18}\text{O}/^{16}\text{O}$ in Arcturus

Molecular bands of $^{12}\text{C}^{18}\text{O}$ could be observed in the modelled spectral region. We estimated the ratio $^{18}\text{O}/^{16}\text{O}$ from a comparison of the relative strength of $^{12}\text{C}^{16}\text{O}$ and $^{12}\text{C}^{18}\text{O}$ isotopologues. To estimate the abundance of a given isotopologue we determine the relative number density of the given species: $X_{^{12}\text{C}^{18}\text{O}} = N_{^{12}\text{C}^{18}\text{O}}/N_{\text{total}(\text{CO})}$, where $N_{\text{total}(\text{CO})}$ is the total number density of all CO isotopologues. For the solar case, $X_{^{12}\text{C}} = 0.989$, $X_{^{13}\text{C}} = 0.011$, and $X_{^{16}\text{O}} = 0.99762$, $X_{^{18}\text{O}} = 0.00200$, see De Bievre & Taylor (1993).

Our value of $X_{^{18}\text{O}} = 0.0005 \pm 0.0004$ was obtained at the min S computed for different spectral ranges in the observed spectrum listed in the upper panel of Fig. 3. On the other hand, a synthetic spectrum generated with the ‘solar’ $X_{^{18}\text{O}}$ gives features which are notably absent from or too weak to be seen in the observed spectrum, see the $^{12}\text{C}^{18}\text{O}$ features marked by arrows at lower panel of Fig. 3, which provides an estimation ‘by eye’ of the lower abundance of ^{18}O in the atmosphere of Arcturus compared to the Sun.

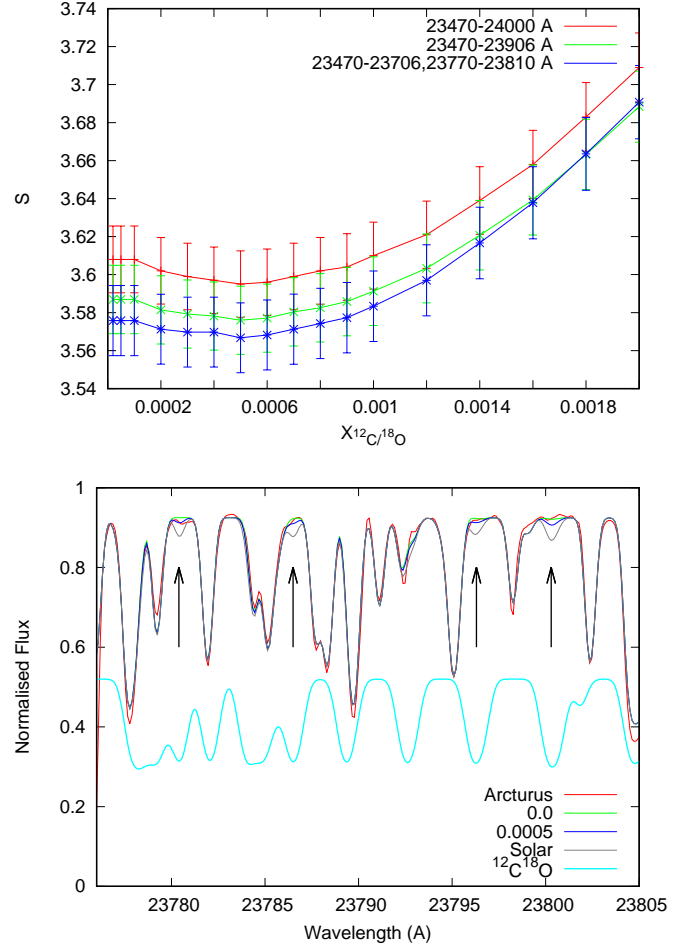


Fig. 3. *Upper panel:* Dependence of the minimisation parameter computed for different spectral ranges on $X_{^{12}\text{C}^{18}\text{O}}$. *Lower panel:* Best fit to the observed spectrum computed for $X_{^{12}\text{C}^{18}\text{O}} = 0.0001$. Profile of the $^{12}\text{C}^{18}\text{O}$ band is shown, in arbitrary units, by a thick cyan line. Vertical arrows mark the $^{12}\text{C}^{18}\text{O}$ features in the computed and observed spectrum.

4.4. $^{17}\text{O}/^{16}\text{O}$ in Arcturus

A similar procedure was used to estimate the ratio $^{17}\text{O}/^{16}\text{O}$ in the atmosphere of Arcturus, see Fig. 4; for the Sun we have $X_{^{17}\text{O}} = 0.00038$ (De Bievre & Taylor 1993). We have some evidence that the fraction of ^{17}O is also lower in the Arcturus. However, this estimation is harder than that for ^{18}O as determination of the abundance of ^{17}O in stellar atmospheres by fitting to observed spectra is hindered by the coincidence between the wavelengths of the band heads of the first overtone of $^{12}\text{C}^{17}\text{O}$ band heads with those of the abundant $^{12}\text{C}^{16}\text{O}$, see Fig. 1. Differences in these spectra increases with the wavelength, however, at the longer wavelength, we observe more complex spectral features created by a large number of CO bands. The pollution by telluric lines also increases to the red spectral region. Taking into account all these factors we may assume that $X_{^{12}\text{C}^{17}\text{O}} < 0.0002$, see upper panel of Fig. 4. However the formal error here is large ± 0.0004 .

4.5. $^{14}\text{C}/^{12}\text{C}$ in Arcturus

Goorvitch (1994) and Li et al. (2015) both computed line lists for the radioactive carbon monoxide isotopologues

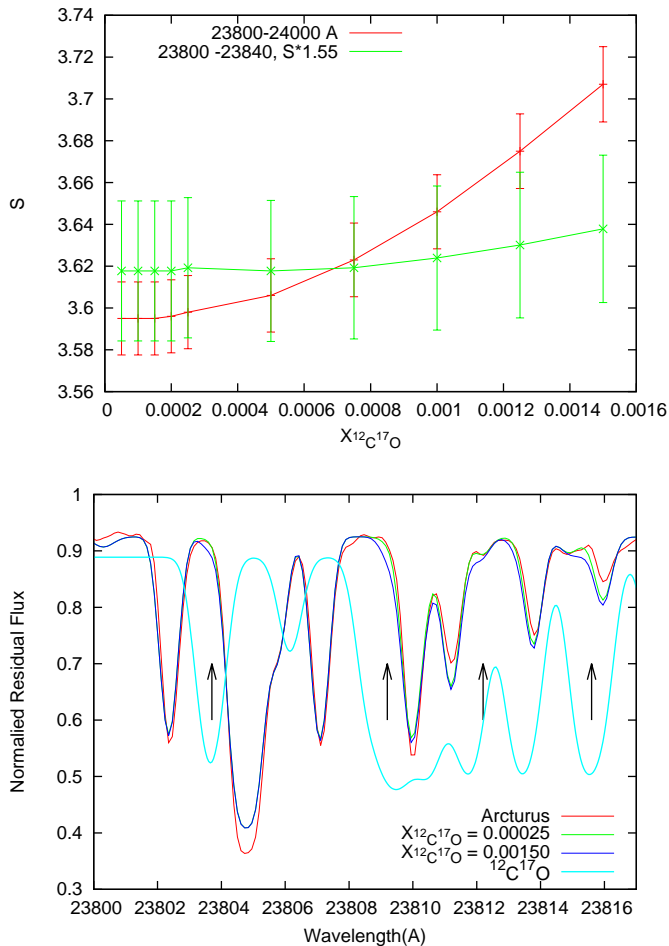


Fig. 4. *Upper panel:* Dependence of the minimisation parameter computed for different spectral ranges on $X_{12C^{17}O}$. *Lower panel:* Comparison of the best fit to the observed spectrum computed for $X_{12C^{17}O} = 0.00025$ and 0.00150 . Thick cyan line shows $^{12}C^{17}O$ features at these wavelength, with the intensity arbitrary scale. Vertical arrows mark the positions of $^{12}C^{17}O$ features in the computed and observed spectrum.

$^{14}C^{16}O$, $^{14}C^{17}O$ and $^{14}C^{18}O$. Radioactive carbon's isotope ^{14}C can be formed in thermonuclear events on the stellar surface. ^{14}C has a half-life of $5,700 \pm 40$ years,¹ and decays by emitting an electron and an electron antineutrino while one of the neutrons in the ^{14}C atom decays to a proton into a stable (non-radioactive) isotope ^{14}N atom. Unfortunately, $^{14}C^{16}O$ bands are shifted redwards with respect to other CO isotopologues, which complicates their analysis due to stronger blending by lines of other bands in this region, see Fig. 1.

Naturally, most ^{14}C in the atmosphere of the star should be in the form of the molecule $^{14}C^{16}O$. We searched for $^{14}C^{16}O$ in the spectrum of Arcturus across 23 900–24 000 Å, in the spectral range containing the head of $v' = 0$ band of the molecule with negative result, no lines of $^{14}C^{16}O$ in the spectrum were found. From our modelling we may conclude that $X_{14C^{16}O} < 0.00025$, see upper panel of Fig. 5 where the position of the $^{14}C^{16}O$ band head computed for $X_{14C^{16}O} = 0.01$, is marked by the arrow in the lower panel of Fig. 5 where we show the theoretical spectrum computed with $X_{14C^{16}O} = 0.2$. The abundance of $X_{14C^{16}O}$

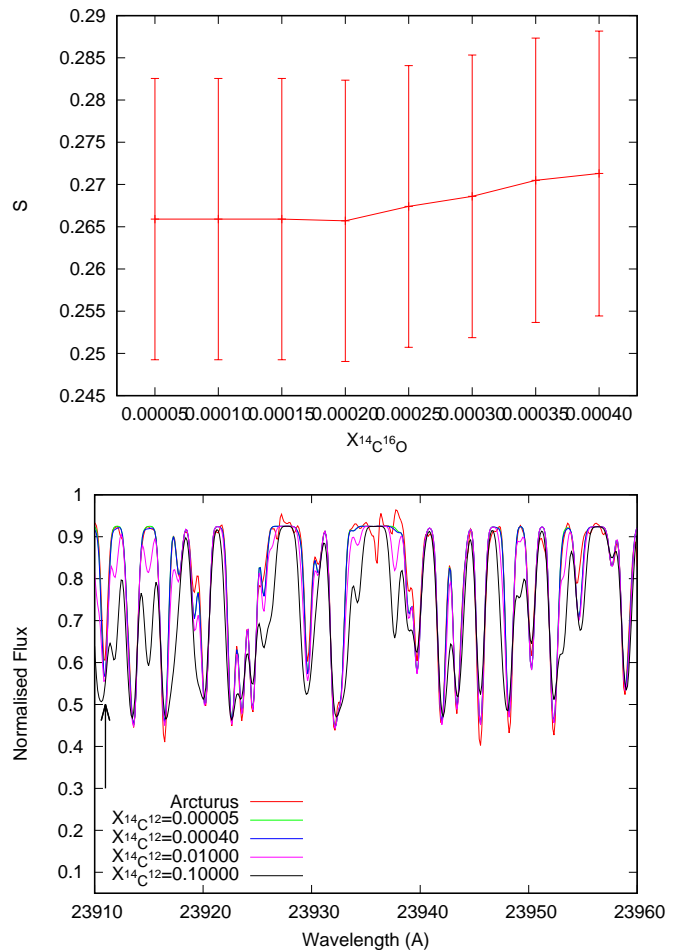


Fig. 5. *Upper panel:* Minimisation parameter S computed for different $X_{14C^{16}O}$. *Lower panel:* Best fit to the observed spectrum computed for $X_{14C^{16}O} = 0.0005$ and 0.00040 . Fits with values $X_{14C^{16}O} = 0.01$ and 0.1 are shown only for the evaluation purposes. The arrow at 23911 \AA marks the position of the head of the $\Delta v = 2, v' = 0$ band of the $^{14}C^{16}O$ molecule. Black thick lines mark missed spectral features of telluric spectrum.

seems to be lower than our detectable limit or the molecule is completely absent in the atmosphere of Arcturus.

4.6. SiO first overtone bands in spectrum HD196610

HD196610 is a variable red giant of $T_{\text{eff}} = 3500 \pm 30 \text{ K}$, see more details in Pavlenko (2019). In a recent paper Pavlenko (2019) performed an initial fit to the observed first overtone bands of SiO in the spectrum of the red giant HD196610 to determine isotopic ratios of silicon in its atmosphere. Unfortunately, Pavlenko (2019) uses an inconsistent convention for the nuclear spin statistical weights. We note that the factor $g_s = 2I + 1 = 1$ for the isotopologous $^{28}\text{Si}^{16}\text{O}$ and $^{30}\text{Si}^{16}\text{O}$, while for $^{29}\text{Si}^{16}\text{O}$ $g_s = 2$ (see Table 1). In this paper we revise the isotopic ratios of Si in the atmosphere of HD196610 by consistently using the ‘astrophysics’ convention.

Furthermore, here we use a more sophisticated procedure than in Pavlenko (2019) to determine the silicon isotopic ratios; the same as was used for the analysis of the CO isotopologues, see Section 4.2. Here, the minimization of χ^2 was performed on a 2D grid of $X_{28\text{Si}^{16}\text{O}}$ and $X_{29\text{Si}^{16}\text{O}}$, at

¹ see http://www.nucleide.org/DDEP_WG/Nuclides/C-14_com.pdf

Table 2. Relative isotopologue abundances of Si obtained from the fits to the first overtone bands of SiO observed in the atmosphere of HD196610. ‘Solar’ isotopic ratios of Si (De Bievre & Taylor 1993) are shown as well.

Star	[Si]	^{28}Si	^{29}Si	^{30}Si	Refs.
The Sun (5770/4.44/0.0)	0.0	0.92	0.05	0.03	[1]
HD196610 (3500/1.0/0.0)	0.0	0.95	0.02	0.03	[2]
HD196610 (3500/1.0/0.0)	-0.2	0.83	0.13	0.04	[3]
HD196610 (3500/1.0/-0.3)	-0.3	0.87	0.10	0.03	[3]
HD196610 (3500/0.5/0.0)	-0.3	0.86	0.11	0.03	[3]
HD196610 (3500/0.5/-0.3)	-0.4	0.89	0.10	0.01	[3]

each point of the grid $X_{30\text{Si}^{16}\text{O}} = 1 - X_{29\text{Si}^{16}\text{O}} - X_{28\text{Si}^{16}\text{O}}$. In this way we were able to determine the ratios for all three isotopologues of SiO.

It is worth noting that the determination of the min of S was carried out iteratively, by varying the total abundance of silicon in the atmosphere of the star, which represents another improvement on the procedure of Pavlenko (2019).

A comparison of results is shown in Table 2. The upper panel of Fig. 6 shows the best fit to the observed spectrum containing the first overtone bands of SiO obtained with the parameters listed in Table 2.

Interestingly, in the case of determination of silicon abundance together with isotopic ratio we obtain similar results for fits that start with different Si abundances (and gravities). Namely, we obtained $[\text{Si}] = -0.3 \pm 0.1$, see Table 2. We thus confirm the result of McDonald et al. (2016). Accuracy of $^{28}\text{Si}^{16}\text{O}$ abundance determination $X_{28\text{Si}^{16}\text{O}} = 0.86 \pm 0.03$ is naturally limited by the low resolution of the observed spectra. Nevertheless, we obtained here non-solar isotopic ratios for Si for all input parameters tested.

As we see from a comparison with the results of Pavlenko (2019), the isotopic ratio computed with a consistent convention for the statistical weights and partition functions changes the SiO isotopologue abundances significantly.

5. Conclusion

There are several line lists for the CO isotopologues available in the literature computed by different authors. In this paper we apply these line lists to analyse the observed spectrum of the red giant Arcturus and show that all provide very similar results. However, the minimisation factor S is lower for the line lists of Goorvitch (1994) and HITEMP2010 than for the newer Li et al. (2015) line list which has been adopted by HITRAN, despite a more sophisticated approach used to generate the latter line list. The detailed analysis of the differences is beyond the scope of this paper, here we note only, the difference in the minimisation parameters S obtained in the framework of the same procedure is clearly caused by the use of the different line lists. On the other hand, the $^{12}\text{C}/^{13}\text{C}$ ratios determined

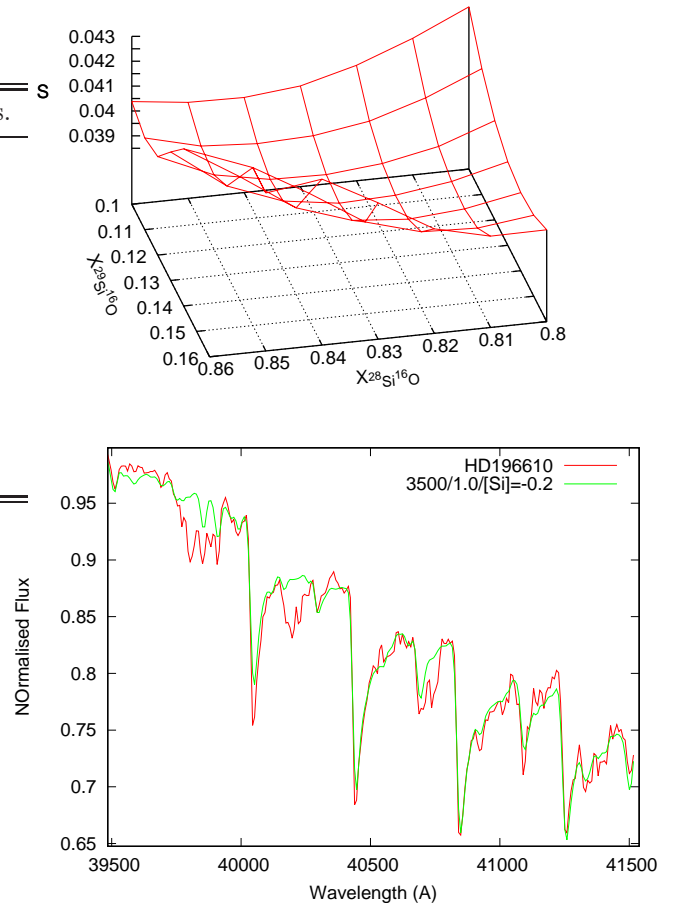


Fig. 6. *Upper panel:* Minimisation parameter S computed on a grid of $X_{28\text{Si}^{16}\text{O}}$ and $X_{29\text{Si}^{16}\text{O}}$, here $[\text{Si}] = -0.2$. *Lower panel:* Best fit to the observed spectrum for $[\text{Si}] = -0.2$, $X_{28\text{Si}^{16}\text{O}} = 0.830$ and 0.13 , respectively. Other ‘‘best solutions’’ are given in the Table 2.

by the best fit to the observed spectrum are the same for all three line lists.

In other words, a consistent usage of the statistical weight convention leads to the perfect agreement for the carbon abundance and isotopic ratios between HITEMP2010 (Rothman et al. 2010) and the line lists of Goorvitch (1994). However, minimisation factor S determined from the χ^2 fit to observed spectrum for the cases of Goorvitch (1994) and Rothman et al. (2010) lists is notably smaller in comparison with the case of Li et al. (2015) line list.

The result of our carbon isotopic determination from fits to the observed spectrum of Arcturus agrees, at least within the error bars, with the previous results by Briley et al. (1994), Pavlenko (2003), and Abia et al. (2012). However, we find that the actual isotopologue abundance determined in the atmosphere of Arcturus depends on the carbon abundance adopted, see Fig. 2. We obtained the isotopic ratio $^{12}\text{C}/^{13}\text{C} = 10 \pm 2$ and the carbon abundance $\log N(\text{C}) = -3.78$ in the framework of our self-consistent approach, in which both $^{12}\text{C}/^{13}\text{C}$ and $\log N(\text{C})$ vary in the process of finding the solution.

We find that the abundance of $^{12}\text{C}^{17}\text{O}$ $X_{12\text{C}^{18}\text{O}} = 0.0004$ in the atmosphere of Arcturus is lower than that in the

Sun, i.e., $X_{12\text{C}^{18}\text{O}} = 0.002$, see De Bièvre & Taylor (1993). Arcturus is an older star than the Sun, so this may be interpreted as the evidence of a lower production of ^{18}O at early epochs, see discussion in Abia et al. (2012) for more details.

Using the fit of our synthetic spectra computed for the set of input parameters of HD196610, e.g. silicon abundances and gravities we determined isotopic ratios in the atmosphere of the star. The abundances and isotopic ratios were determined in the framework of self-consistent approach, when isotopic ratios and abundance of Si vary in the process of determination of the best solution. In that way we found $[\text{Si}] = -0.3 \pm 0.1$, the result agrees with recent estimation of McDonald et al. (2016), obtained using very different procedure. Furthermore, we showed that a) the Si abundance determination show rather marginal dependence on the input parameters, e.g. abundances and gravity of the star, adopted in our work; b) we obtained "non-solar" isotopic ratio of Si in atmosphere of HD196610, c) our estimations of $X_{28\text{Si}} = 0.86 \pm 0.03$ and $X_{29\text{Si}} = 0.86 \pm 0.01$, see Table 2, shows rather marginal dependence on the adopted abundances and gravities, as well.

However, we should note that these estimations were obtained by fits of our synthetic spectra to the spectra of the first overtone SiO bands obtained with rather low resolution. Naturally, more confidence in any analysis of the isotope ratios could be obtained using spectra of better quality; and a more refined analysis should be followed by a detailed abundance analysis to reduce the number of free parameters.

Nevertheless, we demonstrate the importance of the consistent usage of spectroscopic data via a critical revision of the recent results by Pavlenko (2019) on the Si isotopic ratios. This leads to the difference of by a factor more than 2 for $^{29}\text{Si}^{16}\text{O}$, from the nearly solar ratio $^{28}\text{Si}:^{29}\text{Si}:^{30}\text{Si} = 0.92:0.05:0.03$ to the 'non-solar' ratio $0.83:0.13:0.03$. In this paper we also used a more advanced procedure to determine the silicon abundance and its isotopic ratios in the framework of our self-consistent approach, in which both parameters vary in the iteratively process of finding solution.

And finally, it can be assumed with a high degree of confidence that, in the case of these two stars, we observe differences in the isotopic composition of oxygen and silicon between the times and places of their formation and the present day values. Indeed, the masses of both stars are 0.6 and 1.1 solar masses for HD196610 (McDonald et al. 2016) and Arcturus (Ayres & Johnson 1977), respectively. Definitely these masses are not high enough to initiate nucleosynthesis of silicon and oxygen. Detailed analysis of spacial distributions of isotopes in our Galaxy is of crucial importance and vital for modern astrophysics, but the problem is beyond the scope of this paper.

Acknowledgements

This study was funded as part of the routine financing program for institutes of the National Academy of Sciences of Ukraine. Spectroscopic data calculated by the ExoMol group (funded by ERC as part of the Advanced Investigator 267219 project and UK Science and Technology Research Council (STFC) No. ST/R000476/1), the SIMBAD database (CDS, Strasbourg, France), and the Gaia spacecraft data (European Space Agency) were used. This study

is based in part on archival data obtained using the infrared telescope operated by the University of Hawaii under a cooperative agreement with NASA. Authors would like to thank the SAO/NASA ADS team for the development and support of this remarkable data system. We thank the anonymous referee for a thorough review and we highly appreciate the comments and suggestions, which significantly contributed to improving the quality of the paper.

References

- Abia, C., Palmerini, S., Busso, M., & Cristallo, S. 2012, *A&A*, 548, A55
- Anders, E. & Grevesse, N. 1989, *Geochim. Cosmochim. Acta*, 53, 197
- Asplund, M., Grevesse, N., Sauval, A. J., & Scott, P. 2009, *ARA&A*, 47, 481
- Ayres, T. R. & Johnson, H. R. 1977, *ApJ*, 214, 410
- Banerjee, D. P. K., Joshi, V., Evans, A., et al. 2018, *Monthly Notices of the Royal Astronomical Society*, 481, 806
- Barton, E. J., Yurchenko, S. N., & Tennyson, J. 2013, *MNRAS*, 434, 1469
- Bernath, P. F. 2015, *Spectra of Atoms and Molecules*, 3rd edn. (Oxford University Press)
- Böhm-Vitense, E. 1992, *Introduction to Stellar Astrophysics*
- Briley, M. M., Smith, V. V., & Lambert, D. L. 1994, *ApJ*, 424, L119
- Coughlan, G. R. & Fowler, W. A. 1988, *Atomic Data and Nuclear Data Tables*, 40, 283
- Cesetti, M., Pizzella, A., Ivanov, V. D., et al. 2013, *A&A*, 549, A129
- Charbonnel, C. & Zahn, J. P. 2007, *A&A*, 467, L15
- Chase, M. W. & et al. 1985, *J. Phys. Chem. Ref. Data*, 14
- Clayton, D. D. 1983, *Principles of stellar evolution and nucleosynthesis*
- Coxon, J. A. & Hajigeorgiou, P. 2004, *The Journal of chemical physics*, 121, 2992
- Coxon, J. A. & Hajigeorgiou, P. 2013, *Journal of Quantitative Spectroscopy and Radiative Transfer*, 116, 75–78
- De Bièvre, P. & Taylor, P. 1993, *International Journal of Mass Spectrometry and Ion Processes*, 123, 149
- de Vicente, P., Bujarrabal, V., Díaz-Pulido, A., et al. 2016, *A&A*, 589, A74
- Evans, A., Pavlenko, Y. V., Banerjee, D. P. K., et al. 2019, *MNRAS*, 486, 3498
- Gamache, R. R., Roller, C., Lopes, E., et al. 2017, *J. Quant. Spectrosc. Radiat. Transf.*, 203, 70
- González Delgado, D., Olofsson, H., Kerschbaum, F., et al. 2003, *A&A*, 411, 123
- Goorvitch, D. 1994, *ApJS*, 95, 535
- Gordon, I. E., Rothman, L. S., Hill, C., et al. 2017, *J. Quant. Spectr. Rad. Transf.*, 203, 3
- Hinkle, K., Wallace, L., & Livingston, W. 1995, *PASP*, 107, 1042
- Hirschi, R. 2014, *Astrophysics and Space Science Library*, 157–198
- Irwin, A. W. 1981, *ApJS*, 45, 621
- Iwagami, N., Hashimoto, G. L., Ohtsuki, S., Takagi, S., & Robert, S. 2015, *Planet. Space Sci.*, 113, 292
- Knacke, R. F., Gaustad, J. E., Gillett, F. C., & Stein, W. A. 1969, *ApJ*, 155, L189
- Li, G., Gordon, I. E., Rothman, L. S., et al. 2015, *ApJS*, 216, 15
- McDonald, I., Zijlstra, A. A., & Boyer, M. L. 2012, *MNRAS*, 427, 343
- McDonald, I., Zijlstra, A. A., Sloan, G. C., et al. 2016, *MNRAS*, 456, 4542
- Nakamura, T., Umeda, H., Nomoto, K., Thielemann, F.-K., & Burrows, A. 1999, *ApJ*, 517, 193
- Palmerini, S., La Cognata, M., Cristallo, S., & Busso, M. 2011, *ApJ*, 729, 3
- Pavlenko, Y. V. 1997, *Astronomy Reports*, 41, 537
- Pavlenko, Y. V. 2003, *Astronomy Reports*, 47, 59
- Pavlenko, Y. V. 2008, *Astronomy Reports*, 52, 749
- Pavlenko, Y. V. 2014, *Astronomy Reports*, 58, 825
- Pavlenko, Y. V. 2019, *Kinematics and Physics of Celestial Bodies*, 35, 164
- Peterson, R. C., Dalle Ore, C. M., & Kurucz, R. L. 1993, *ApJ*, 404, 333
- Rayner, J. T., Cushing, M. C., & Vacca, W. D. 2009, *ApJS*, 185, 289
- Rinsland, C. P. & Wing, R. F. 1982, *ApJ*, 262, 201
- Romano, D., Matteucci, F., Zhang, Z. Y., Papadopoulos, P. P., & Ivison, R. J. 2017, *MNRAS*, 470, 401

- Rothman, L., Gordon, I., Barber, R., et al. 2010, *Journal of Quantitative Spectroscopy and Radiative Transfer*, 111, 2139 , xVIth Symposium on High Resolution Molecular Spectroscopy (HighRus-2009)
- Ryabchikova, T., Piskunov, N., Kurucz, R. L., et al. 2015, *Physica Scripta*, 90, 054005
- Ryde, N., Edvardsson, B., Gustafsson, B., et al. 2009, *A&A*, 496, 701
- Sauval, A. J. & Tatum, J. B. 1984, *ApJS*, 56, 193
- Schaefer, L., Lodders, K., & Fegley, B. 2012, *ApJ*, 755, 41
- Snedden, C. 1991, in *IAU Symposium*, Vol. 145, *Evolution of Stars: the Photospheric Abundance Connection*, ed. G. Michaud & A. V. Tutukov, 235
- Tennyson, J. & Yurchenko, S. N. 2012, *MNRAS*, 425, 21
- Tennyson, J., Yurchenko, S. N., Al-Refaie, A. F., et al. 2016, *J. Mol. Spectrosc.*, 327, 73
- Tinetti, G., Drossart, P., Eccleston, P., et al. 2018, *Experimental Astronomy*, 46, 135
- Tobin, T. L., Kemball, A. J., & Gray, M. D. 2019, *ApJ*, 871, 189
- Vlemmings, W. H. T., Humphreys, E. M. L., & Franco-Hernández, R. 2011, *ApJ*, 728, 149
- Wollman, E. R., Geballe, T. R., Greenberg, L. T., Holtz, J. Z., & Rank, D. M. 1973, *ApJ*, 184, L85
- Yoon, D.-H., Cho, S.-H., Kim, J., Yun, Y. j., & Park, Y.-S. 2014, *ApJS*, 211, 15